



Active Contour Models for Boundary Extraction with Application to Medical Images with Noise

Nasrul Azizi Kon¹, Abdul Kadir Jumaat^{1,2,*}, Muhammad Danial Adzlizan Suhaizi¹

¹ School of Mathematical Sciences, College of Computing, Informatics and Mathematics, Universiti Teknologi MARA, 40450 Shah Alam, Malaysia

² Institute for Big Data Analytics and Artificial Intelligence (IBDAAI), Universiti Teknologi MARA, 40450 Shah Alam, Malaysia

ARTICLE INFO

Article history:

Received 23 June 2023

Received in revised form 5 October 2023

Accepted 18 October 2023

Available online 5 November 2023

Keywords:

Active contour; boundary extraction;
medical images

ABSTRACT

In medical image processing, active contour model is a method used to segment or extract the boundaries of an image for further processing. Recently, a selective active contour model called Selective Segmentation with Chessboard Distance (SSCD) model has been proposed to effectively segment a particular object in an image. However, the SSCD model has problems in extracting noisy images, which may result in poor segmentation. It is known that the presence of noise in some medical images cannot be avoided and can lead to poor segmentation. The aim of this research is therefore to reformulate the SSCD model to segment some medical images with noise. The modification is done by considering two different image denoising algorithms, the Gaussian filter and the bilateral filter, as new fitting terms in the SSCD model, resulting in two variants of modified SSCD models, referred to as SSCDG and SSCDB, respectively. The accuracy of the segmented image was evaluated using the Jaccard (JSC) and Dice similarity coefficient (DSC). Numerical experiments showed that the proposed SSCDG model based on the Gaussian filter denoising algorithm has the highest JSC and DSC values, which means the highest segmentation accuracy compared to the SSCD and SSCDB models. In the future, the proposed model can be extended to three-dimensional and color formulations.

1. Introduction

Image processing is the process of interpreting and using an image to extract information from it. The aim is to facilitate the interpretation or improve the information of a digital image [1]. The most common task in image processing is image segmentation, which is the technique used to extract the boundaries of an object or divide an image into multiple segments [2-4]. In medicine, image segmentation is used to detect an object in a medical image or to analyze the nature of diseases such as cancer and breast abnormalities [5-10].

Mathematically, given an input image $u(x, y)$ in a bounded domain $D \subset \mathbb{R}^2$, the segmentation method will be partitioning $u(x, y)$ into finite number of intersected and non-overlapped area $D_i, i =$

* Corresponding author.

E-mail address: abdulkadir@tmsk.uitm.edu.my

<https://doi.org/10.37934/araset.33.2.300312>

1,2,...*i*. Image segmentation methods can be classified into 5 categories: Threshold-based segmentation, clustering-based segmentation, artificial neural network-based segmentation, edge-based segmentation and region-based segmentation [11].

Threshold-based segmentation is the most popular method of image segmentation that can be used to convert a multi-layered image into a binary image. It involves selecting a suitable threshold value to divide the image pixels into multiple areas and distinguish objects from the background. Otsu's thresholding method, P-tile method, histogram-dependent approach, edge maximization technique, mean method and visual technique are some of the thresholding strategies that have been presented by various researchers [11]. However, it can be difficult to determine a suitable threshold and the method can be sensitive to image noise.

Clustering-based segmentation is a method that typically illustrates clustering in one of two ways: by partitioning pixels or by grouping pixels [12]. In partitioning, an image is divided into sections that are "labelled" according to a set of criteria. In grouping, pixels are grouped together based on some assumptions that determine how they should preferably be grouped. This method can lead to an unsatisfactory result if the target object is close to a neighboring object.

Artificial neural network-based segmentation consists of interconnected neurons as found in neural networks. To obtain a result, each neuron takes a piece of input data, usually a pixel of an image, and applies a basic calculation called an activation function. Each neuron has a numerical weight that affects the result. The result is fed into more neural layers until at the end of the process the neural network gives a prediction for each input or pixel [11]. This type of method can give good results, but it is too dependent on the amount of data and the process of segmenting images is unknown [13].

Edge-based segmentation is used to find the boundaries of objects in images. Detecting sudden changes or breaks in brightness is the way edge detection is done. The well-known edge detectors like zero crossing, Canny Edge detector, Sobel, Prewitt, Roberts and Laplacian of Gaussian [14] are some of the operators used by the edge detection methods. Similar to threshold-based segmentation, edge-based segmentation can also be sensitive to image noise.

Region-based segmentation is more straightforward compared to edge-based segmentation [15]. Region-based approaches divide an image into similar regions based on a set of predetermined criteria. Well-known examples of region-based segmentation models are region growing, region merging and active contour models. For a digital medical image with low contrast, noisy images and close to normal tissue, region growing and region merging methods may give unsatisfactory results as all features or objects (including image noise) in an image can be segmented by these two methods.

On the other hand, active contour models have proven to be an effective region-based segmentation method. For example, the models derived using a level set framework can adapt to topological changes in an input image and are less sensitive to initialization [16,17]. In this study, we focus primarily on active contour models, which belong to the region-based segmentation methods due to their strengths mentioned above.

The active contour models can be classified into two types, namely global active contour and selective active contour. The global active contour model is a method for segmenting all objects in an image based on certain features. Examples of global segmentation models include [16,18-21]. Although global active contour models are effective for segmenting all objects in digital images, they are less effective for extracting only a specific object in a specific image [3].

Selective segmentation involves the extraction of specific regions and features of the image under consideration [2,3]. This is often used in medical image analysis, for example, to extract anatomical organs or lesions. Examples of effective selective models have been proposed by [17,22-24]. The

most recent model is that of Ref. [3], namely Selective Segmentation based on Chessboard Distance (SSCD).

Abdullah and Jumaat [3] have shown that the SSCD model based on Chessboard distance function performs better in terms of computational time than the model using the quasi-Euclidean distance function and the city block distance function. However, SSCD is not designed to segment images with noise, which can lead to poor segmentation, especially during the acquisition phase of medical imaging where noise in the images cannot be avoided. This shows how important the process of image denoising is for medical image analysis. Noise reduction techniques such as the Gaussian filter and the bilateral filter are commonly used to improve the quality of images.

Therefore, in this paper, we propose selective active contour models for effective segmentation of noisy medical images by reformulating the SSCD model, where the fitting term in the SSCD model is replaced by the commonly used denoising techniques, Gaussian filter and Bilateral filter. The remainder of this paper is structured as follows. In Section 2, we first give an overview of the SSCD model. In the methodology of Section 3, we formulate and solve the proposed models. In Section 4, we present the experimental results. Conclusions and recommendations are given in Section 5.

2. Review on The SSCD Model

The most common distance functions are Euclidean, City Block and Chessboard [25]. In Ref. [25], it is found that the Chessboard distance function gives better results in segmentation with watersheds. Therefore, authors in Ref. [3] have proposed a new selective active contour model for edge extraction based on the Chessboard distance function, the SSCD model. The SSCD model is defined by the following Eq. (1)

$$\min_u \{SSCD(u, c_1, c_2) = \mu \int_D |\nabla u| dD + \lambda \int_D ru dD + \theta \int_D P_c u dD + \alpha \int_\Omega v(u) dD\} \quad (1)$$

The function $r = (z - c_1)^2 - (z - c_2)^2$ is the fitting term where c_1 and c_2 are the average intensity values inside and outside segmented curve $u(x, y)$. Here, $z = z(x, y)$ is a given image in domain $D \subset \mathbb{R}^2$. The positive constants μ, λ, θ and α are determined depending on the input images. The availability of $n_1 (\geq 3)$ points are assumed to form the marker set $M = w_i = (x_i^*, y_i^*) \in D, 1 \leq i \leq n_1$ that defines a polygon. The geometrical point in M is defined as an initial polygonal contour and polygon P is connecting the markers using set B . The first term of the integrand is called as the regularization term to ensure smoothness of the generated segmented curve, $u(x, y)$. The last term $v(u) = H(\sqrt{(2u-1)^2 + \bar{\epsilon}} - 1) [\sqrt{(2u-1)^2 + \bar{\epsilon}} - 1]$ is the penalty function introduced to ensure the solution of u is in between 0 and 1 where $H(x) = 0.5(1 + (2/\pi)\arctan(x/\bar{\epsilon}))$ for small constant $\bar{\epsilon}$. The function $p_c(x, y)$ refers to the Chessboard distance function denoted as the following Eq. (2)

$$P_c(x, y) = \max(|x_1 - x_p|, |y_1 - y_p|) \quad (2)$$

To solve the SSCD model in Eq. (1), the Euler-Lagrange partial differential equation (EL-PDE) with Neumann boundary condition is derived, defined as the following Eq. (3)

$$\mu C(u) - \lambda r - \theta P_c - \alpha v' = 0. \quad (3)$$

Here, the curvature term $C(u) = \nabla \cdot (\nabla u / |\nabla u|)$. Many gradient descent based methods can be used to calculate Eq.(3). In Ref. [3], the authors suggested using the additive operator splitting scheme (AOS) to solve the equation. This model has high potential in many research areas such oil and gas industries [26] for corrosion detection, ultrasound imaging in biofuel production [27] and it can be integrated with artificial neural network [28] for image processing. However, although the SSCD model is effective, it may be sensitive to image noise and therefore give unsatisfactory results in medical image segmentation. Therefore, some modifications of the SSCD model are required to improve its segmentation accuracy. In the next section, the methodology for modifying the SSCD model using image denoising techniques is presented.

3. Methodology

The SSCD model [3] was modified by substituting the fitting term, z in Eq. (1) with the information from the well-known denoising techniques i.e., Gaussian filter and Bilateral filter.

Firstly, we introduce our first proposed model termed SSCDG which is the modification of the SSCD model based on the Gaussian filter, ZG . The modified model is defined as the following Eq. (4)

$$\min_{u, c_1, c_2} \{SSCDG(u, c_1, c_2) = \mu \int_D |\nabla u| dD + \lambda \int_D (ZG - c_1)^2 u dD - \lambda \int_D (ZG - c_2)^2 u dD + \theta \int_D P_c u dD + \alpha \int_D v(u) dD\}. \quad (4)$$

Here, $ZG = e^{-(x^2+y^2)/2\sigma^2}$ where σ^2 is variance around each pixel (x, y) .

Next, we define the second proposed model namely SSCDB. The model is a modified version of SSCD model based on the Bilateral filter, ZB . The SSCDB model is defined as the following Eq. (5)

$$\min_{u, c_1, c_2} \{SSCDB(u, c_1, c_2) = \mu \int_D |\nabla u| dD + \lambda \int_D (ZB - c_1)^2 u dD - \lambda \int_D (ZB - c_2)^2 u dD + \theta \int_D P_c u dD + \alpha \int_D v(u) dD\}. \quad (5)$$

Here, $ZB = \frac{1}{W} \sum_{x_i \in \Omega} z(x_i) f_r(\|z(x_i) - z(x)\|) g_s(\|x_i - x\|)$. The normalization term W is defined as

$W = \sum_{x_i \in \Omega} f_r(\|z(x_i) - z(x)\|) g_s(\|x_i - x\|)$ where z is the input (noisy) image, x are the coordinate of the current pixel to be filtered in the window Ω centered in x , f_r is the range kernel for smoothing differences in intensities and g_s is the spatial kernel for smoothing differences in coordinates.

All the proposed models of Eq. (4) and (5) are solved by solving their associate Euler-Lagrange partial differential equation (EL-PDE). Here, we demonstrate how to derive the EL-PDE for Eq. (4) because the derivation of the EL-PDE for Eq. (5) is mostly the same.

From Eq. (4), we denote that $I_1(u) = |\nabla u| = \sqrt{u_x^2 + u_y^2} = (u_x^2 + u_y^2)^{\frac{1}{2}}$, $I_2(u) = rGu$, $I_3(u) = P_c u$, and $I_4(u) = v(u)$ where $rG = (ZG - c_1)^2 - (ZG - c_2)^2$. Next, we define a small parameter ε which is a real parameter with a range of values around 0 and a test function ϕ . Consequently,

$I_1|u + \varepsilon\phi| = |\nabla(u + \varepsilon\phi)| = \sqrt{(u_x + \varepsilon\phi_x)^2 + (u_y + \varepsilon\phi_y)^2}$. At $\varepsilon = 0$, the derivative of $\sqrt{(u_x + \varepsilon\phi_x)^2 + (u_y + \varepsilon\phi_y)^2}$ with respect to ε is given as

$$\frac{d}{d\varepsilon} \sqrt{(u_x + \varepsilon\phi_x)^2 + (u_y + \varepsilon\phi_y)^2} = \frac{1}{2} [u_x^2 + u_y^2]^{-\frac{1}{2}} \cdot [2u_x\phi_x + 2u_y\phi_y] = \frac{\nabla u \cdot \nabla \phi}{|\nabla u|}.$$

Reviewing the Taylor expansion as an example, consider the function $f(a) = [(x + ac_1)^2 + (y + ac_2)^2]^p$ where $p \neq 0$. The derivative with respect to a is $p[(x + ac_1)^2 + (y + ac_2)^2]^{p-1} (2(x + ac_1)c_1 + 2(y + ac_2)c_2)$. At $a = 0$, the result is $p \frac{(2xc_1 + 2yc_2)}{[x^2 + y^2]^{1-p}}$. The Taylor expansion at $a = 0$ can be defined as the following Eq. (6)

$$f(a) = f(0) + f'(a)a + O(a^2) = (x^2 + y^2)^p + p \frac{(2xc_1 + 2yc_2)}{(x^2 + y^2)^{1-p}} a + O(a^2). \quad (6)$$

Thus, by applying the Taylor expansion in Eq. (6) at $\varepsilon = 0$, the term I_1 can be extended as follows

$$I_1|u + \varepsilon\phi| = |\nabla(u + \varepsilon\phi)| = \sqrt{(u_x + \varepsilon\phi_x)^2 + (u_y + \varepsilon\phi_y)^2} = |\nabla u| + \frac{\nabla u \cdot \nabla \phi}{|\nabla u|} \varepsilon + O(\varepsilon^2).$$

For the second term, $I_2(u) = rGu$, the derivative with respect to ε and at $\varepsilon = 0$ is given as follows

$$\frac{d}{d\varepsilon} (rG(u + \varepsilon\phi)) = rG\phi.$$

Thus, implementing the Taylor expansion in Eq. (6) at $\varepsilon = 0$ gives

$$rG(u + \varepsilon\phi) = rGu + rG\phi\varepsilon + O(\varepsilon^2).$$

As for the third term, $I_3 = P_c u$, the derivative with respect to ε and at $\varepsilon = 0$ is defined as

$$\frac{d}{d\varepsilon} (P_c(u + \varepsilon\phi)) = P_c\phi.$$

Hence, when applying Taylor expansion in Eq. (6) at $\varepsilon = 0$, the term I_3 can be expressed as follows

$$P_c(u + \varepsilon\phi) = P_c u + P_c\phi\varepsilon + O(\varepsilon^2).$$

Similarly, for the fourth term, $I_4(u) = v(u)$, the derivative with respect to ε and at $\varepsilon = 0$ is given as

$$\frac{d}{d\varepsilon}(v(u + \varepsilon\phi)) = v'(u)\phi.$$

Therefore, applying Taylor expansion in Eq. (6) at $\varepsilon = 0$, the term I_4 becomes

$$v(u + \varepsilon\phi) = v(u) + v'(u)\phi\varepsilon + O(\varepsilon^2).$$

The next step is to determine the first variation of the functional SSCDG with respect to u . Therefore, the first variation for $I(u) = I_1 + I_2 + I_3 + I_4$ combined with any test function ϕ will be defined as

$$\lim_{\varepsilon \rightarrow 0} \frac{I(u + \varepsilon\phi) - I(u)}{\varepsilon} = \int_D \left[\mu \frac{\nabla u \cdot \nabla \phi}{|\nabla u|} + \lambda rG\phi + \theta P_c \phi + \alpha v'(u)\phi \right] dD = 0.$$

By using Green's first identity as the following relation, $\int_D \nabla \phi \cdot \vec{\omega} dD = \int_{dD} \phi \vec{\omega} \cdot \vec{\eta} ds - \int_D \phi \nabla \cdot \vec{\omega} dD$, we let

$$\vec{\omega} = \frac{\nabla u}{|\nabla u|} \text{ and obtain } \int_D \nabla \phi \cdot \vec{\omega} dD = \int_D \nabla \phi \cdot \frac{\nabla u}{|\nabla u|} dD = \int_{dD} \phi \frac{\nabla u}{|\nabla u|} \cdot \vec{\eta} ds - \int_D \phi \nabla \cdot \frac{\nabla u}{|\nabla u|} dD.$$

Next, set the boundary condition (Neumann Type) $\nabla u \cdot \vec{\eta} = 0$ we have

$$\int_D \left[-\mu \nabla \cdot \frac{\nabla u}{|\nabla u|} \phi + \lambda rG\phi + \theta P_c \phi + \alpha v'(u)\phi \right] dD = 0.$$

The integrand is equal to zero if

$$-\mu \nabla \cdot \frac{\nabla u}{|\nabla u|} \phi + \lambda rG\phi + \theta P_c \phi + \alpha v'(u)\phi = 0 \Rightarrow \phi \left[-\mu \nabla \cdot \frac{\nabla u}{|\nabla u|} + \lambda rG + \theta P_c + \alpha v'(u) \right] = 0.$$

As a result, the EL-PDE with Neumann boundary condition for all test function ϕ for Eq. (4) is defined as the following Eq. (7)

$$-\mu \nabla \cdot \frac{\nabla u}{|\nabla u|} + \lambda rG + \theta P_c + \alpha v'(u) = 0. \tag{7}$$

Using a similar process, the EL-PDE for SSCDB defined in Eq. (5) is defined as the following Eq. (8)

$$-\mu \nabla \cdot \frac{\nabla u}{|\nabla u|} + \lambda rB + \theta P_c + \alpha v'(u) = 0. \tag{8}$$

Here, $rB = (ZB - c_1)^2 - (ZB - c_2)^2$. Next, Eq. (7) and (8) can be solved iteratively using many approaches such as the finite difference scheme, the optimization multilevel scheme or the operator splitting scheme. In this study, we applied the additive operator splitting (AOS) scheme, a similar method used by Ref. [3] to solve the SSCD model. The details of the AOS scheme are explained in detail in Ref. [29].

The following algorithm shows the steps to implement the newly proposed SSCDG model to calculate the solution using MATLAB software.

Algorithm 1: Algorithm to solve the proposed SSCDG model

1. Use command 'imread' in MATLAB to import the image.
2. Set the parameter values of α , μ , θ , λ and define the marker set M .
3. Compute the solution of ZG .
4. Initialize $n=0$, thus $u^{(0)}$.
5. For $iter = 1$ to maximum iterations, $maxit$ or $\|u^{n+1} - u^n\| / \|u^n\| \leq tol$ do
 Calculate the average intensity values $c_1^{(n)}$ and $c_2^{(n)}$.
 Calculate $f^{(n)} = \lambda rG + \theta P_c + \alpha v'$.
 Update $u^{(n)} \leftarrow \min_u SSCDG(c_1^{(n)}, c_2^{(n)}, \alpha^{(n)})$ to $u^{(n+1)}$ using AOS scheme.
 end for
6. $u \leftarrow u^{(n)}$. The output u will be defined as the final solution.

Here, we have the value of tolerance, $tol = 1 \times 10^{-5}$ and the maximum iteration ($maxit$) is 5000 iterations. By changing ZG to ZB in Step 3, a similar process is repeated for the implementation of the second proposed model, SSCDB.

4. Results and Discussion

In this study, thirty (30) medical images of size 128 x 128 were collected from Ref. [30] with added noise. The images are ultrasound images that contain breast abnormalities. For each test image, the ground truth segmentation solution is provided by the online database. We will segment the images using the existing model, SSCD and the proposed models, SSCDG and SSCDB. The value of $\mu=1$, $\alpha=2$, $\lambda=0.01$ are fixed for all problems. The value of θ varies between 1000 to 2000 depending on the images. The segmentation accuracy of all models will be evaluated using Jaccard Similarity Coefficient (JSC) and Dice Similarity Coefficient (DSC) defined as $JSC = |S_n \cap S_g| / |S_n \cup S_g|$ and $DSC = |S_n \cap S_g| / (|S_n| + |S_g|)$ where S_n is the segmented result and S_g is the ground truth solution. The range of return value of the similarity function is in between 0 (poor segmentation accuracy) and 1 (perfect segmentation accuracy). Figure 1 shows the sample of 3 (out of 30) test images which are *Img1*, *Img5* and *Img21*.

Based on Figure 1, the set markers and the initial contour are indicated by the green dots and the yellow line in the first row. The second row shows the benchmark solution (ground truth). For illustration, we show in the following Figure 2 the segmentation results for the test images from Figure 1 (*Img1*, *Img5* and *Img21*) with SSCD, SSCDG and SSCDB.

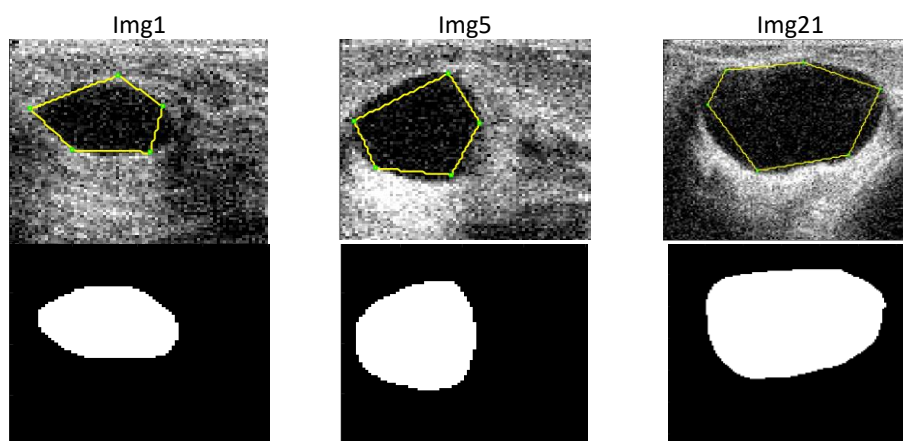


Fig. 1. Sample of test images with markers and initial contour (first row) and ground truth (second row)

Based on Figure 2, the binary results for SSCD, SSCDG and SSCDB are shown in the segmentation of *Img1* in the second row by *Img1a*, *Img1b* and *Img1c* respectively. The segmentation results can also be viewed in the curve plot, as shown in the fourth row. Similarly, the sixth and eighth rows show the results for all methods in the binary and curve plots when segmenting the test image *Img5*. The results for segmenting the test image *Img21* for all methods are displayed in the tenth and the second last rows.

By visual observation, all modified models are able to extract the boundaries of the target object, except for the original model SSCD, where the noisy part within the target object is also segmented (over-segmented). Moreover, the final results for the proposed models SSCDG and SSCDB are less noisy than SSCD. To quantitatively evaluate the overall segmentation accuracy, we calculate the JSC and DSC values for all 30 test images as shown in Table 1 below.

Table 1 shows that the SSCDG model achieved the highest average JSC value. The average JSC value for the SSCDG model is 0.7148. The lowest JSC value is obtained by the SSCD model for the majority of the problems. The average JSC value for the SSCD model is 0.6992. The SSCDB model has an average JSC value of 0.7049. In summary, the SSCDG model segmented the test images better than the other models. A similar pattern can be observed for the DSC value, where the SSCDG model achieved the highest average DSC value of 0.8322 compared to the other models. On the other hand, the SSCD model scored the lowest DSC value for the majority of the problems, with the average DSC value for the SSCD model being 0.8196. The average DSC value for the SSCDB model is 0.8223.

This experiment shows that the proposed SSCDG model and the SSCDB model based on the Gaussian filter and the Bilateral filter respectively, are more suitable for the segmentation of noisy medical images. This is due to the image filtering property in the formulation of the two proposed models, which is able to reduce image noise, contributing to higher segmentation accuracy. However, we found that SSCDG gives slightly higher accuracy compared to SSCDB. The main reason for this is the noise distribution in the images, which is of the Gaussian type. We note that the Gaussian noise is the most frequent type of noise that occurs in real images. This gives an advantage to SSCDG, which is based on the Gaussian filtering approach. We therefore recommend the SSCDG model for segmentation of noisy medical images.

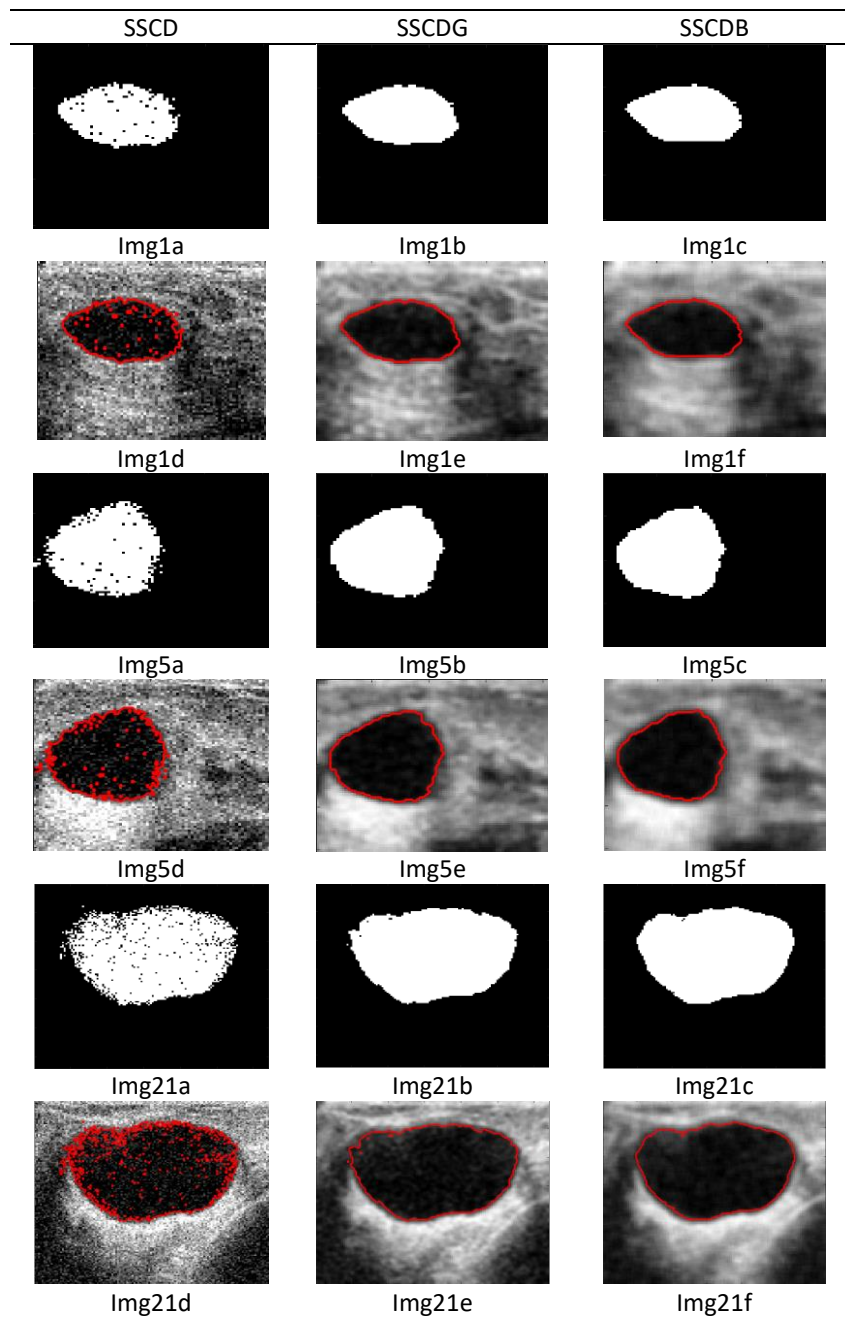


Fig. 2. The binary and curve representation results for SSCD, SSCDG and SSCDB in segmenting Img1, Img5 and Img21

Table 1
 The JSC and DSC values of all models for all test images

Test image	JSC			DSC		
	SSCD	SSCDG	SSCDB	SSCD	SSCDG	SSCDB
Img1	0.8218	0.8399	0.8369	0.9022	0.913	0.9112
Img2	0.6393	0.5323	0.5323	0.7800	0.6947	0.6947
Img3	0.5833	0.5931	0.5931	0.7368	0.7446	0.7446
Img4	0.6898	0.7216	0.7053	0.8164	0.8383	0.8272
Img5	0.8705	0.8982	0.8922	0.9308	0.9464	0.9430
Img6	0.8128	0.8372	0.8363	0.8967	0.9114	0.9109
Img7	0.7056	0.6976	0.6935	0.8274	0.8219	0.8190
Img8	0.6829	0.7113	0.7088	0.8116	0.8313	0.8296
Img9	0.7142	0.7647	0.7179	0.8333	0.8664	0.8358
Img10	0.6290	0.7749	0.7722	0.7722	0.8726	0.8714
Img11	0.6226	0.6060	0.6667	0.7674	0.7547	0.8000
Img12	0.7411	0.7569	0.7487	0.8513	0.8617	0.8563
Img13	0.7846	0.8296	0.8051	0.8793	0.9068	0.8921
Img14	0.7770	0.6189	0.5874	0.8745	0.7638	0.7401
Img15	0.6239	0.6391	0.6325	0.7684	0.7798	0.7749
Img16	0.5806	0.6561	0.6538	0.7346	0.7923	0.7907
Img17	0.6394	0.6720	0.6644	0.78	0.8938	0.7984
Img18	0.7006	0.7473	0.7294	0.8239	0.8554	0.8435
Img19	0.6989	0.6237	0.5914	0.8228	0.7682	0.7432
Img20	0.6340	0.6447	0.6078	0.7760	0.7840	0.7561
Img21	0.8392	0.8855	0.8784	0.9126	0.9393	0.9353
Img22	0.6860	0.6900	0.7127	0.8137	0.8166	0.8322
Img23	0.7500	0.8097	0.8084	0.8571	0.8948	0.8940
Img24	0.6206	0.5474	0.5366	0.7659	0.7075	0.6984
Img25	0.8091	0.8640	0.8495	0.8945	0.9270	0.9186
Img26	0.6238	0.6335	0.6068	0.7683	0.7756	0.7553
Img27	0.5009	0.5303	0.5105	0.6675	0.6931	0.6759
Img28	0.5894	0.6743	0.6621	0.7417	0.8055	0.7967
Img29	0.8282	0.8282	0.8496	0.906	0.9060	0.9187
Img30	0.7763	0.8155	0.7578	0.8740	0.8983	0.8622
Average	0.6992	0.7148	0.7049	0.8196	0.8322	0.8223

We are also interested in testing the sensitivity of the parameter θ . The value of θ is important to ensure the selective property of the proposed SSCDG model in segmenting the target object. To demonstrate the effect on the segmentation result of the SSCDG model, we chose the test image Img30. Figure 3 shows the segmentation results for the SSCDG model with different values θ for the test image Img30.

The first column of Figure 3 shows the test image with the markers set and the initial curve. The segmentation results for the test image Img30 using the values of $\theta=1$, $\theta=1500$ and $\theta=50000$ are shown in the second, third and fourth columns respectively. The segmentation results clearly show that the test image is over-segmented when $\theta=1$ because the SSCDG model segments the nearby healthy tissue around the target instead of extracting only the boundary line of the target. At $\theta=1500$, the SSCDG model is able to segment the boundary line of the target object. However, for a large value of $\theta=50000$, the segmentation result has the shape of a polygon, which is the initial curve for the segmentation of the test image Img30. This experiment shows the limitations of our proposed models where the value of θ is determined by trial and error. As a general guideline, the value of θ is large for objects that are close to image noise or normal tissue, while a smaller value of θ is required for smooth objects.

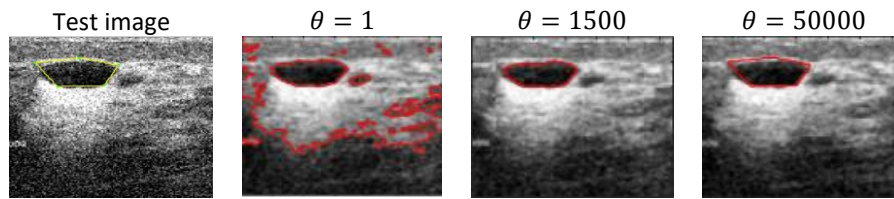


Fig. 3. Segmentation results with different value of θ ($\theta = 1$, $\theta = 1500$ and $\theta = 50000$)

5. Conclusions

The focus of this research is to extract the boundaries of the target object in a noisy medical image using an active contour based selective segmentation model. Since the existing model SSCD has its limitations in processing noisy images, two modified versions of the model were proposed in this study, namely SSCDG and SSCDB. The modification was done by introducing an image denoising algorithm in the formulation. To solve the proposed models, we first establish the Euler-Lagrange partial differential equation for each of the modified models and solved using the Additive Operator Splitting (AOS) scheme. Numerical experiments are conducted to compare the performances of the original and modified models and were analysed using JSC and DSC.

The results of JSC and DSC values show that most of the modified models have improvements in terms of segmentation accuracy compared to the original model SSCD. The results showed that the SSCDG provided better quality of the denoised image and consequently the segmentation accuracy was higher compared to the other models. The original SSCD model provided the lowest accuracy. This is because the formulation of the SSCD model does not include an image filtering property to reduce image noise. As a result, it was found that the original SSCD model segments too much, considering the noisy part of the images as the target object, which reduces the segmentation accuracy. We found that the proposed SSCDG model gives slightly higher accuracy compared to the SSCDB model. This is due to the Gaussian distribution of noise in the images, which gives an advantage to the SSCDG model based on the Gaussian filtering approach. Therefore, the recommended model in this study is the SSCDG model.

When testing parameter sensitivity, we found that the parameter θ used in the SSDG model plays an important role. The parameter was selected manually or by trial-and-error principle depending on the input image. Thus, this is the major limitation of the proposed SSDG model.

For further studies, the recommended model i.e., SSCDG model can be extended to other applications like food image processing. It can also be reformulated into a three-dimensional and it can be extended into a vector-valued formulation for colour image segmentation. This is because vector-valued (colour) and three-dimensional images have rich information and distinct intensity that can be helpful in analysing medical or non-medical images.

Acknowledgement

This work was supported by the Ministry of Higher Education (MOHE) and Universiti Teknologi MARA, Shah Alam, grant number FRGS/1/2021/STG06/UITM/02/3.

References

- [1] Torres, Helena R., Pedro Morais, Bruno Oliveira, Cahit Birdir, Mario Rüdiger, Jaime C. Fonseca, and João L. Vilaça. "A review of image processing methods for fetal head and brain analysis in ultrasound images." *Computer Methods and Programs in Biomedicine* 215 (2022): 106629. <https://doi.org/10.1016/j.cmpb.2022.106629>
- [2] Mohd Ghani, Noor Ain Syazwani, Abdul Kadir Jumaat, and Rozi Mahmud. "Boundary extraction of abnormality region in breast mammography image using active contours." *ESTEEM Academic Journal* 18 (2022): 115-127.

- [3] Abdullah, Siti Aminah, and Abdul Kadir Jumaat. "Selective image segmentation models using three distance functions." *Journal of Information and Communication Technology* 21, no. 01 (2022): 95-116. <https://doi.org/10.32890/10.32890/jict2022.21.1.5>
- [4] Mohd Ghani, Noor Ain Syazwani, and Abdul Kadir Jumaat. "Selective Segmentation Model for Vector-Valued Images." *Journal of Information and Communication Technology* 21, no. 02 (2022): 149-173. <https://doi.org/10.32890/jict2022.21.2.1>
- [5] Zaman, Nur Atiqah Kamarul, Wan Eny Zarina Wan Abdul Rahman, Abdul Kadir Jumaat, and Siti Salmah Yasiran. "Classification of breast abnormalities using artificial neural network." In *AIP Conference Proceedings*, vol. 1660, no. 1. AIP Publishing, 2015. <https://doi.org/10.1063/1.4915671>
- [6] Jumaat, Abdul Kadir, Siti Salmah Yasiran, Aminah Abdul Malek, Wan Eny Zarina WA Rahman, Norzaituleha Badrin, Siti Hajar Osman, Siti Rohaina Rafiee, and Rozi Mahmud. "Performance comparison of Canny and Sobel edge detectors on Balloon Snake in segmenting masses." In *2014 International Conference on Computer and Information Sciences (ICCOINS)*, pp. 1-5. IEEE, 2014. <https://doi.org/10.1109/ICCOINS.2014.6868368>
- [7] Jumaat, Abdul K., Wan E. Rahman, Arsmah Ibrahim, Siti S. Yasiran, Rozi Mahmud, and Aminah A. Malek. "Masses characterization based on angular margin measurement." In *2012 Fourth International Conference on Computational Intelligence, Modelling and Simulation*, pp. 265-269. IEEE, 2012. <https://doi.org/10.1109/CIMSim.2012.50>
- [8] Jumaat, Abdul Kadir, Wan Eny Zarina WA Rahman, Arsmah Ibrahim, and Rozi Mahmud. "Segmentation and characterization of masses in breast ultrasound images using active contour." In *2011 IEEE International Conference on Signal and Image Processing Applications (ICSIPA)*, pp. 404-409. IEEE, 2011. <https://doi.org/10.1109/ICSIPA.2011.6144126>
- [9] Yasiran, Siti Salmah, Abdul Kadir Jumaat, Aminah Abdul Malek, Fatin Hanani Hashim, Nor Dhaniah Nasrir, Syarifah Nurul Azirah Sayed Hassan, Normah Ahmad, and Rozi Mahmud. "Microcalcifications segmentation using three edge detection techniques." In *2012 IEEE International Conference on Electronics Design, Systems and Applications (ICEDSA)*, pp. 207-211. IEEE, 2012. <https://doi.org/10.1109/ICEDSA.2012.6507798>
- [10] Yasiran, Siti Salmah, Abdul Kadir Jumaat, Mazani Manaf, Arsmah Ibrahim, WAR Wan Eny Zarina, Aminah Malek, Mohamed Faris Laham, and Rozi Mahmud. "Comparison between GVF snake and ED snake in segmenting microcalcifications." In *2011 IEEE International Conference on Computer Applications and Industrial Electronics (ICCAIE)*, pp. 597-601. IEEE, 2011. <https://doi.org/10.1109/ICCAIE.2011.6162204>
- [11] Jeevitha, K., A. Iywaraya, V. RamKumar, S. Mahaboob Basha, and V. Praveen Kumar. "A review on various segmentation techniques in image processing." *European Journal of Molecular & Clinical Medicine* 7, no. 4 (2020): 1342-1348.
- [12] Sarma, Rituparna, and Yogesh Kumar Gupta. "A comparative study of new and existing segmentation techniques." In *IOP conference series: materials science and engineering*, vol. 1022, no. 1, p. 012027. IOP Publishing, 2021. <https://doi.org/10.1088/1757-899X/1022/1/012027>
- [13] Lee, Lay Khoon, Siau Chui Liew, and Weng Jie Thong. "A review of image segmentation methodologies in medical image." In *Advanced Computer and Communication Engineering Technology: Proceedings of the 1st International Conference on Communication and Computer Engineering*, pp. 1069-1080. Springer International Publishing, 2015. https://doi.org/10.1007/978-3-319-07674-4_99
- [14] Puri, Saurav, and Surender Singh. "Image Segmentation Techniques: A Survey." *International Journal of Engineering and Applied Physics* 1, no. 2 (2021): 127-135.
- [15] Abdulateef, Salwa Khalid, and Mohanad Dawood Salman. "A Comprehensive Review of Image Segmentation Techniques." *Iraqi Journal for Electrical & Electronic Engineering* 17, no. 2 (2021). <https://doi.org/10.37917/ijeee.17.2.18>
- [16] Zhi, Xu-Hao, and Hong-Bin Shen. "Saliency driven region-edge-based top down level set evolution reveals the asynchronous focus in image segmentation." *Pattern Recognition* 80 (2018): 241-255. <https://doi.org/10.1016/j.patcog.2018.03.010>
- [17] Jumaat, Abdul K., and Ke Chen. "A reformulated convex and selective variational image segmentation model and its fast multilevel algorithm." *NUMERICAL MATHEMATICS-THEORY METHODS AND APPLICATIONS* 12, no. 2 (2018): 403-437. <https://doi.org/10.4208/nmtma.OA-2017-0143>
- [18] Fang, Lingling, Tianshuang Qiu, Yin Liu, and Chaofeng Chen. "Active contour model driven by global and local intensity information for ultrasound image segmentation." *Computers & Mathematics with Applications* 75, no. 12 (2018): 4286-4299. <https://doi.org/10.1016/j.camwa.2018.03.029>
- [19] Zhao, Wencheng, Xianze Xu, Yanyan Zhu, and Fengqiu Xu. "Active contour model based on local and global Gaussian fitting energy for medical image segmentation." *Optik* 158 (2018): 1160-1169. <https://doi.org/10.1016/j.jilleo.2018.01.004>

- [20] Iqbal, Ehtesham, Asim Niaz, Asif Aziz Memon, Usman Asim, and Kwang Nam Choi. "Saliency-driven active contour model for image segmentation." *IEEE Access* 8 (2020): 208978-208991. <https://doi.org/10.1109/ACCESS.2020.3038945>
- [21] Girija, S. P., A. Akhila, D. Deepthi, R. Uday Kiran, and P. Abinay Krishna. "Saliency and Transmission Feature Extraction from Underwater Images Using Level Set Method." In *2022 First International Conference on Electrical, Electronics, Information and Communication Technologies (ICEEICT)*, pp. 1-7. IEEE, 2022. <https://doi.org/10.1109/ICEEICT53079.2022.9768472>
- [22] Jumaat, A. K., and K. Chen. "Three-dimensional convex and selective variational image segmentation model." *Malaysian Journal of Mathematical Sciences* 14, no. 3 (2020): 437-450.
- [23] K Jumaat, Abdul, and Ke Chen. "Fast algorithm for selective image segmentation model." *International Journal of Engineering & Technology* 7, no. 4.33 (2018): 41-41. <https://doi.org/10.14419/ijet.v7i4.33.23481>
- [24] Chen, K., and A. Jumaat. "An Optimization Based Multilevel Algorithm for Variational Image Segmentation Models." *Electronic Transactions on Numerical Analysis* 46 (2017): 474-504.
- [25] Chen, Qing, Xiaoli Yang, and Emil M. Petriu. "Watershed segmentation for binary images with different distance transforms." In *Proceedings of the 3rd IEEE international workshop on haptic, audio and visual environments and their applications*, vol. 2, pp. 111-116. 2004.
- [26] Shafie, Nur Liyana, and Roslina Mohammad. "Safeguard and mitigation of hazard and operability during simultaneous production and drilling at oil and gas platform." *Progress in Energy and Environment* (2023): 39-49. <https://doi.org/10.37934/progee.23.1.3949>
- [27] Lee, Kiat Moon, and Ka Nyan Ng. "Effect of Ultrasonication in Organosolv Pretreatment for Enhancement of Fermentable Sugars Recovery from Palm Oil Empty Fruit Bunches." *Progress in Energy and Environment* (2019): 15-23.
- [28] Yagoub, Sami Abdelrahman Musa, Gregorius Eldwin Pradipta, and Ebrahim Mohammed Yahya. "Prediction of bubble point pressure for Sudan crude oil using Artificial Neural Network (ANN) technique." *Progress in Energy and Environment* (2021): 31-39.
- [29] Spencer, Jack, and Ke Chen. "A convex and selective variational model for image segmentation." *Communications in Mathematical Sciences* 13, no. 6 (2015): 1453-1472. <https://doi.org/10.4310/CMS.2015.v13.n6.a5>
- [30] Rodtook, Annupan, Khwunta Kirimasthong, Wanrudee Lohitvisate, and Stanislav S. Makhanov. "Automatic initialization of active contours and level set method in ultrasound images of breast abnormalities." *Pattern Recognition* 79 (2018): 172-182. <https://doi.org/10.1016/j.patcog.2018.01.032>